ACS OMEGA

http://pubs.acs.org/journal/acsodf

Article

Effects of Water-Soluble Sodium Compounds on the Microstructure and Combustion Performance of Shengli Lignite

Yanjun Wang,[†] Yunfei Zhao,[†] Runxia He,* Zhenghao Yan, Xuemei Li, Huacong Zhou, Na Li, Keduan Zhi, Yinmin Song, Yingyue Teng, and Quansheng Liu*

Cite This: *ACS Omega* 2021, 6, 24848−24858

Read Online

ACCESS | Metrics & More | Article Recommendations

ABSTRACT: Different water-soluble sodium compounds (NaCl, Na_2CO_3, and NaOH) were used to treat Shengli lignite, and the resulting effects on the microstructure and combustion performance of the coal were investigated. The results showed that Na_2CO_3 and NaOH had a significant impact on combustion performance of lignite, while NaCl did not. The Na_2CO_3-treated lignite showed two distinct weight-loss temperature regions, and after NaOH treatment, the main combustion peak of the sample moved to the high temperature. This indicates that both Na_2CO_3 and NaOH can inhibit the combustion of lignite, with the latter showing a greater effect. The FT-IR/XPS results revealed that Na^+ interacted with the oxygen-containing functional groups in lignite to form a "−COONa" structure during the Na_2CO_3 and NaOH treatments. It is deduced that the inhibitory effect on combustion of lignite may be attributed to the stability of the "−COONa" structure, and the relative amount is directly correlated with the inhibitory effect. The XRD/Raman analysis indicated that the stability of the aromatic structure containing "−COOH" increased with the number of "−COONa" structures formed. Additionally, experiments with carboxyl-containing compounds further demonstrated that the number of oxygen-containing functional groups combined with Na was the main reason for the differences in the combustion performance of treated lignite.

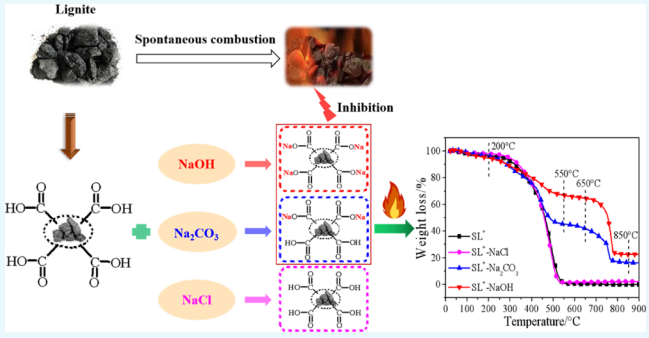

1. INTRODUCTION

Low-rank coal makes up a large proportion of China's coal reserves. As a typical low-rank coal, the development and utilization of lignite, which has large reserves, occurred relatively late.[1,2] In addition to a complex structure, well-developed voids, and a high water content, lignite contains much higher amounts of volatile matter and oxygen-containing functional groups.[3−5] These compositional and structural characteristics make it remarkably easy for lignite to react with oxygen during the processes of mining, storage, and transportation. If the heat from this reaction cannot be discharged in time, it can result in spontaneous combustion,[6] which not only wastes coal resources but also greatly limits the effective utilization of lignite. Therefore, it is crucial to select appropriate treatment methods to inhibit the spontaneous combustion of lignite.

To date, there has been plenty of literature on the topic of inhibiting the spontaneous combustion of coal,[7,8] such as through sorting and stacking coal with different particle sizes, as well as reducing the stacking height, which can extend the spontaneous combustion cycle of coal and reduce the risk of spontaneous combustion.[9] Cheng et al.[10] reported a smart gel with good thermal stability as well as good adhesion and swelling properties at high temperature. This type of gel can be used to inhibit the spontaneous combustion of coal by covering its surface, thereby significantly reducing not only the temperature of the fire source, but also the heat and CO generated from the combustion. Alternatively, chemical treatment methods are often used to change the composition of coal and consume its surface-active sites, thereby reducing the heat released during combustion. Some inhibitors, such as NaCl, $MgCl_2$, and $CaCl_2$, can effectively prevent contact between the coal and oxygen, as well as remove some of the heat accumulated during spontaneous combustion.[11−14] However, due to the flow of air and moisture evaporation, it is difficult to maintain the long-term inhibitory effect.[15] Other inhibitors include oxidants such as permanganate, perchlorate, and peroxide,[16] ionic liquids,[17−19] and inorganic salts such as Na_3PO_4 and $Mg(Ac)_2$.[20] The inhibitors can interact with active

Received: July 13, 2021
Published: September 16, 2021

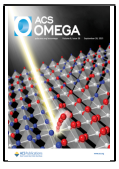

functional groups on the coal surface to reduce the number of active groups or inhibit free radical reactions. However, due to the complexity of the coal structure, different coal types have different distributions of functional groups,[21] which, to a large extent, is overlooked by the existing literature. Chemical inhibitors also suffer from certain other disadvantages; for example, when combined with certain types of coals, their inhibitory effects may become unstable,[22] and some are likely to cause undesirable chemical contamination.[23]

Alongside the aforementioned inhibitors, treatment with alkaline compounds such as NaOH has been widely employed as an efficient chemical purification method for lignite, as it can significantly alter the structural characteristics of lignite. This includes modifying the pore distribution on the coal surface, reducing the specific surface area, and removing some of the oxygen-containing functional groups and minerals in the coal, which reduces environmental pollution.[24] Moreover, alkaline treatment can reduce the reactivity and increase the ignition temperature of lignite.[25,26] The alkaline treatment methods reported in the literature mostly used NaOH, with the Na contained therein playing a key role; hence, the status of sodium in lignite will directly affect its thermochemical reaction performance. For instance, the pyrolysis performance of Victoria lignite was mainly affected by the presence of sodium carboxylate.[27,28] Most of the sodium in Australian high-salt coal exists in the form of water-soluble NaCl, and there is also a large amount of sodium carboxylate present, with a decomposition temperature range of 500−550 °C.[29] As an alkali metal ion, the sodium ion can exchange with lignite to form a sodium carboxylate structure that will affect the pyrolysis behavior of the coal.[27,28] The sodium in coal from Wucai Bay, Xinjiang in China mainly exists in the form of water-soluble sodium compounds and the organic sodium present therein mainly exists in the form of carboxylate. The composition of water-soluble and organic sodium in this coal varies under the effects of pyrolysis temperature.[30] When the coal was mixed with aqueous solutions of NaAc and $NaHCO_3$, the alkalinity of the solution was enhanced and the "−COONa" structure was detected in the coal, indicating that this structure inhibits the decomposition of oxygen-containing groups during pyrolysis.[31] In addition, the combination of alkali metal ions with organic carboxylic acids as small molecules can lead to enhanced thermal stability. For instance, when using sodium, potassium, and magnesium to react with benzoic acid, it was found that the alkali and alkaline earth metals resulted in the formation of thermally stable carboxylates with decomposition temperatures >400 °C.[32]

A previous study by the authors of this paper[33] found that in the process of treating Shengli lignite with NaOH, the sodium ions interacted with the oxygen-containing functional groups in lignite to form a carboxylate-like structure. It is speculated that the formation of such a structure inhibits the lignite's combustion performance.[28,32] It is worth noting that alkali treatment not only affects the types of specific functional groups in lignite but can also change the number of functional groups within it and have a significant impact on its thermochemical reaction characteristics. For instance, the stability of monosodium terephthalate (NaTP) and disodium terephthalate (Na_2TP) formed by the reaction between NaOH and the carboxyl groups in terephthalic acid (TP) has been found to be enhanced. The difference in the number of functional groups bound to sodium results in different stabilities between NaTP and Na_2TP, with the former having a much lower decomposition temperature (320 °C) than the latter (640 °C).[34] Additionally, from the results of a research work,[33] it was found that, compared to the untreated Shengli lignite, combustion hysteresis appears after treatment with alkali solutions, with the hysteresis phenomenon becoming more pronounced with increasing alkali concentration. However, Wang et al.[35] studied the effect of different NaOH concentrations on the oxidation behavior of lignite at low temperatures (<200 °C) and found that treatment using high NaOH concentrations significantly reduced the content of reactive functional groups and inhibited the oxidation behavior of coal, whereas using low NaOH concentrations increased the tendency of the coal toward spontaneous combustion. Similarly, other studies[36−38] investigated the tendency toward spontaneous combustion of Victoria lignite coal samples by kneading the coal with hydroxides of different alkali and alkaline earth metals under the action of an external force to make them denser and more homogenized. The results indicated that high NaOH concentrations reduced the tendency toward spontaneous combustion due to the strong electrostatic interactions with the coal, and that the inhibitory effect of the hydroxides of different alkali and alkaline earth metals on the spontaneous combustion of the lignite is in the order $Ca(OH)_2$ < KOH < NaOH. Low NaOH concentrations, however, can catalyze the spontaneous combustion by destroying the hydrogen bond network and inhibiting the cross-linking reaction. Although these studies have confirmed that NaOH in sufficient concentrations can interact with carboxyl functional groups to produce carboxylates with high thermal stability, lower concentrations of NaOH will result in different or even completely opposite effects on the oxidation and combustion properties of coal. This may be due to the structural complexity of lignite. Therefore, it is necessary to further study the mechanisms by which sodium acts in the alkali treatment process as well as the effects of the amount of bonded state (−COONa) groups on the lignite's structure and combustion performance.

Previous studies have mainly focused on the effect of NaOH treatment on the low-temperature oxidation and combustion characteristics of lignite, and there is consequently less literature regarding the treatment of lignite with water-soluble sodium compounds. Based on the aforementioned literature and previous experimental results, the present study aims to investigate the effects of treatment with various water-soluble sodium compounds, namely NaCl, Na_2CO_3, and NaOH, on the microstructure and combustion reaction performance of Shengli lignite. The structures of the prepared coal samples were characterized using scanning electron microscopy/energy dispersive X-ray spectroscopy (SEM−EDS), Fourier-transform infrared spectroscopy (FT-IR), X-ray photoelectron spectroscopy (XPS), X-ray powder diffraction (XRD), Raman spectroscopy, and other methods in order to analyze the changes in the main active functional groups. Thermogravimetric analysis (TGA) was used to investigate the effects of the different water-soluble sodium compounds on the combustion performance of the lignite. Carboxyl-containing compounds were also used to simulate lignite, which further illustrated the effect of the bonded state (−COONa) groups on the structure and combustion performance of lignite. It is hoped that this research will provide valuable insights into preventing the spontaneous combustion of lignite coal and toward the safe and effective utilization of lignite.

https://doi.org/10.1021/acsomega.1c03695
ACS Omega 2021, 6, 24848−24858

2. EXPERIMENTAL SECTION

2.1 Preparation of Coal Samples. The lignite samples used in this study, labeled as SL, were obtained from the Shengli coalfield in Inner Mongolia, China. The samples were crushed and sieved. The samples with a particle size of 0.150−0.180 mm were selected for further treatment.

For the experiments, the lignite was ground to obtain a fine powder with a particle size of 0.075−0.150 mm, and then dried (105 °C, 4 h). In order to eliminate the influence of minerals during the experiment, the lignite was demineralized using hydrochloric acid- and hydrofluoric acid-leaching techniques prior to the experiments, as follows: first, SL was mixed with 18.5% HCl at a ratio of 1 g: 10 mL (coal/solution) with stirring at room temperature for 24 h. The slurry was vacuum filtered, further washed continuously with deionized water until the filtrate contains no Cl^-, and dried at 105 °C for 4 h. The resulting sample was denoted as SLM. SLM was mixed with HF at a ratio of 1 : 6 (w/v) and stirred for 24 h. The mixture was rinsed repeatedly with deionized water until the filtrate contains no F^- ($CaCl_2$). Finally, the demineralized solid sample was dried, and denoted as SL^+.

ICP (inductively coupled plasma-optical emission spectrometry system, Optima 7000, PerkinElmer) was used to determine the main metal ions of the inherent minerals of lignite as shown in Table 1. Compared to SL, the content of metal ions in SL^+ was significantly lower, confirming that most of the inherent minerals within the latter were leached by HCl and HF, the sodium component dropped from 0.58 to 0.00%, and almost all the sodium component was eluted.

Table 1. Metal Ion Content in the Coal Samples

	content/wt %						
samples	Al^{3+}	Na^+	Ca^{2+}	Si^{4+}	Fe^{n+}	K^+	Mn^{n+}
SL	2.40	0.58	0.41	3.11	0.11	0.08	0.06
SL^+	0.11	0.00	0.01	0.14	0.00	0.00	0.00
SL^+-NaCl	0.14	0.01	0.03	0.15	0.00	0.00	0.00
SL^+-Na_2CO_3	0.12	5.62	0.02	0.14	0.00	0.00	0.00
SL^+-NaOH	0.13	6.48	0.01	0.17	0.00	0.00	0.00

SL^+ was added separately to 1 mol/L solutions of three water-soluble sodium compounds—NaCl, Na_2CO_3, and NaOH—in a ratio of 1 g: 10 mL, and the resulting slurries were stirred at room temperature for 4 h, then filtered and further washed with distilled water. This rinsing procedure was repeated until the pH of the filtrate became constant. The obtained solids were placed in an oven at 105 °C to dry for 4 h. The samples were denoted as SL^+-NaCl, SL^+-Na_2CO_3, and SL^+-NaOH, respectively. The results from the main metal ions, and from proximate and ultimate analyses of the tested samples are presented in Tables 1 and 2. Table 1 shows that the Na content in SL^+-NaCl was almost 0.0%, while the Na contents in SL^+-Na_2CO_3 and SL^+-NaOH were 5.62 and 6.48%, respectively. Table 2 shows that the ash content in SL^+-NaCl changed little relative to SL^+, while the ash content in SL^+-Na_2CO_3 and SL^+-NaOH increased by about 14 and 21% relative to SL^+. Ultimate analysis shows that the carbon content of the samples after NaCl and Na_2CO_3 treatment decreased slightly, and the oxygen content increased slightly, while the carbon content of the sample after NaOH treatment increased, and the oxygen content decreased. The content of other elements did not change much.

2.2 NaOH Treatment of Carboxylic Compounds. Trimesic acid (TMA) was used as the carboxylic compound. A certain amount of TMA was mixed in a stoichiometric ratio with NaOH solutions of different concentrations (1, 2, and 3 mol/L). The solutions were stirred for a certain period of time until well mixed, then dried at 105 °C to obtain the samples, which were labeled as STMA-1, STMA-2, and STMA-3.

2.3 Characterization of Coal Samples. For the SEM−EDS measurements, a Phenom ProX field emission electron microscope equipped with an energy dispersive X-ray spectrometer (Phenom-World, Netherlands) was used to test the surface morphologies and perform semiquantitative microchemical analysis of the coal samples. The acceleration voltage, magnification, and resolution of the instrument were 5−15 kV, 80−150,000×, and 2.5 nm, respectively.

The FT-IR spectra were recorded with the KBr pellet technique using a NEXUS 6700 infrared spectrometer (Nicolet, USA). The detection range was from 4000 to 400 cm^{-1} with a resolution of 4 cm^{-1}.

For XPS measurements, an ESCALAB 250Xi instrument (Thermo Fisher Scientific, USA) was used. The X-ray source was an Al Kα target, and the energy range and calibration standard used were 0−1350 eV and C 1s, respectively (284.6 eV).

The XRD measurements were performed on a SmartLab 9 kW instrument (Rigaku, Japan) equipped with a highly sensitive D/teX Ultra 250 detection system and Cu Kα radiation (45 kV, 200 mA). Powder XRD patterns of the samples were recorded from 5 to 90° in the 2θ range. The scanning speed was 2°/min.

Raman spectroscopy was performed on an inVia microscope (Renishaw, UK). The laser wavelength was 532 nm and the power of the laser was 0.3 mW. The spectrum was recorded in the range of 120−4000 cm^{-1}.

2.4 Combustion Performance (TGA) Tests. A HCT-4 simultaneous thermal analyzer (Beijing Hengjiu, China) was used to test the combustion performance of the coal samples, with the experimental procedure as follows: 15−20 mg of the sample was placed at the bottom of an alumina crucible. The heating rate was set at 10 °C/min, and the temperature was in

Table 2. Proximate and Ultimate Analyses of the Base SL^+ and Treated Samples[a]

	proximate analysis (wt %)			ultimate analysis(wt %, daf)				
samples	A_d	V_{daf}	FC_d	C	H	N	S	O*
SL	10.97	43.25	50.52	64.69	4.02	1.00	2.03	28.26
SL^+	0.79	46.17	53.41	69.74	4.38	0.96	1.64	23.28
SL^+-NaCl	1.35	45.18	54.08	67.24	4.37	0.98	1.53	25.88
SL^+-Na_2CO_3	15.72	50.82	41.45	66.28	5.00	0.98	1.51	26.23
SL^+-NaOH	21.48	46.68	41.87	72.71	5.73	0.97	1.67	18.92

[a]d, dried basis. daf, dried ash-free basis.* by difference.

https://doi.org/10.1021/acsomega.1c03695
ACS Omega 2021, 6, 24848−24858

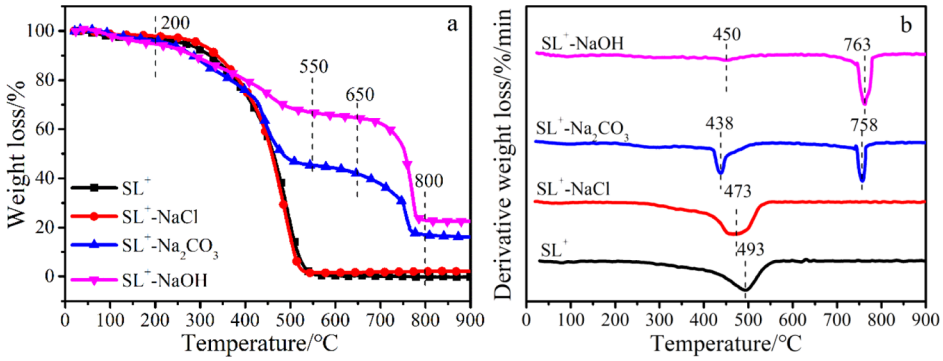

Figure 1. Combustion properties of the base SL^+ and treated samples: (a) TG; (b) DTG.

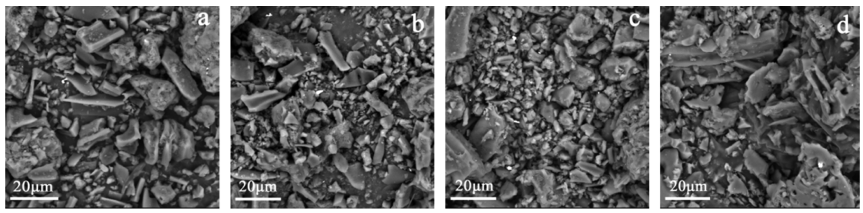

Figure 2. SEM micrographs of (a) SL^+, (b) SL^+-NaCl, (c) SL^+-Na_2CO_3, and (d) SL^+-NaOH.

the range from ambient to 900 °C. The air flow rate during the experiment was set at 100 mL/min.

3. RESULTS AND DISCUSSION

3.1. Treatment of Lignite with Soluble Sodium-Containing Compounds. *3.1.1. Combustion Performance.* Figure 1 shows the TG/DTG curves of base SL^+ as well as the samples treated with soluble sodium-containing compounds. As the figure shows, the combustion performance of SL^+-NaCl was close to that of SL^+, whereas those for SL^+-Na_2CO_3 and SL^+-NaOH were significantly different. Figure 1a shows that the weight-loss temperature region of the SL^+ and SL^+-NaCl coal samples was 200−600 °C, whereas SL^+-Na_2CO_3 and SL^+-NaOH had weight-loss temperature ranges of 200−550 °C and 650−800 °C, respectively. As Figure 1b shows, the maximum combustion rate of SL^+ occurred at 493 °C. After being treated with NaCl, this temperature slightly shifted to a lower value. However, the SL^+-Na_2CO_3 and SL^+-NaOH samples showed different behaviors, for the former, with their weight loss mainly concentrated in two temperature ranges, these ranges corresponded to maximum combustion rates at 438 °C and 758 °C, respectively, whereas for the latter, the weight loss was almost entirely concentrated within the second temperature range, which had a maximum combustion rate at 763 °C. It is considered that the reactions before 500 °C were caused by the combustion of the inherent organic structure in the coal sample, while the reactions occurring in the range of 700−800 °C mainly corresponded to the combustion or decomposition of the "−COONa" structure formed by the action of sodium and carboxyl functional groups in the coal sample. Figure 1a also shows that the residual ash of SL^+ and SL^+-NaCl was not significantly different, indicating the Na-containing component was not retained in the coal samples. However, the residual ash after combustion of SL^+-Na_2CO_3 and SL^+-NaOH was about 16 and 22% higher, respectively, than that of SL^+, indicating the presence of Na-containing components in the two coal samples. Moreover, the content of the Na-containing component in SL^+-NaOH was higher than that in SL^+-Na_2CO_3. This was basically consistent with the results shown in Tables 1 and 2. These results indicate that the neutral NaCl does not significantly alter the combustion properties of SL^+, whereas the weakly alkaline Na_2CO_3 and strongly alkaline NaOH solutions do, with the latter producing a more obvious change following treatment.

3.1.2 SEM−EDS Analysis. Figure 2 shows the SEM images of the base SL^+ and treated samples. As the figure shows, the SL^+ sample had a lamellar structure with irregular edges and greater numbers of larger-sized particles. Following NaCl treatment, the number of larger-sized particles decreased and that of smaller-sized particles increased, while exhibiting a structure similar to SL^+. In SL^+-Na_2CO_3, the number of small particles increased further, and a slight agglomeration phenomenon was observed. SL^+-NaOH, on the other hand, showed more obvious agglomeration, with some blocks being denser. EDS analysis of the coal samples (Table 3) reveals that

Table 3. EDS Results for the Base SL^+ and Treated Samples

samples	elemental composition/wt %				
	C	O	N	S	Na
SL^+	69.63	27.29	2.32	0.76	0
SL^+-NaCl	68.67	27.85	2.80	0.68	0
SL^+-Na_2CO_3	64.78	26.08	3.04	0.58	5.52
SL^+-NaOH	66.13	24.25	2.87	0.35	6.40

no sodium was present in the coal samples after NaCl treatment, but sodium was present in the Na_2CO_3- and NaOH-treated samples. Additionally, the weight percent of Na in SL^+-NaOH was higher than that of SL^+-Na_2CO_3, this was consistent with the ICP characterization results. These results indicate that the coal samples treated with NaCl solution do not retain any sodium, whereas those treated with the Na_2CO_3 and NaOH solutions do, with the sodium content of the latter being higher.

3.1.3 FT-IR Analysis. The variations in functional groups of the treated coal samples were mainly concentrated in the

https://doi.org/10.1021/acsomega.1c03695
ACS Omega 2021, 6, 24848−24858

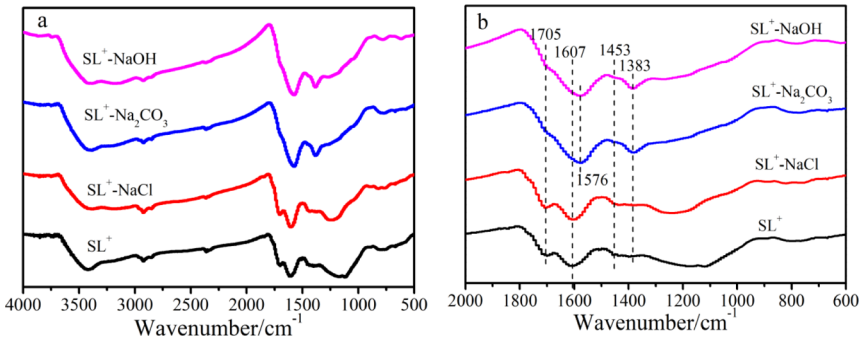

Figure 3. FT-IR spectra of the base SL^+ and treated samples in the wavenumber ranges of (a) 4000−500 and (b) 2000−600 cm^{-1}.

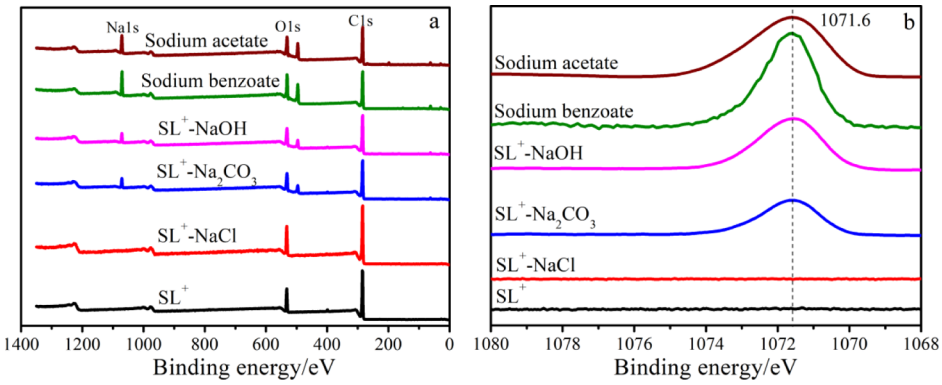

Figure 4. XPS spectra of the base SL^+ and treated samples: (a) full spectra; (b) Na 1s spectra.

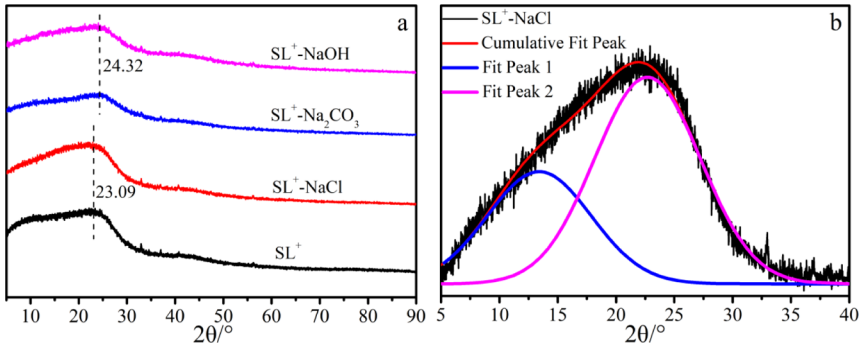

Figure 5. XRD patterns of the base SL^+ and treated samples: (a) XRD patterns of coal samples; (b) peak-fitting diagram for SL^+-NaCl.

2000−600 cm^{-1} wavenumber range (Figure 3b). The peak at 1705 cm^{-1} was attributed to the symmetrical stretching vibrations of −C═O in the carboxyl group.[32] SL^+ showed an obvious absorption peak at this position, which did not change significantly following NaCl treatment. However, the adsorption peak was significantly weakened after Na_2CO_3 and NaOH treatment, indicating that both of these compounds can reduce the number of carboxyl groups in coal samples. In addition, the absorption peak at 1607 cm^{-1} for both SL^+ and SL^+-NaCl, which is attributed to the asymmetric stretching vibration of −COO, shifted to 1576 cm^{-1} for SL^+- Na_2CO_3 and SL^+-NaOH, and the symmetric stretching vibration absorption peak of −COO appeared at 1383 cm^{-1}.[33] The relatively strong asymmetric stretching vibrations in the wavenumber range of 1610−1550 cm^{-1} and the relatively weak symmetric stretching vibrations near 1400 cm^{-1} confirm the presence of carboxylate.[32,39] Owing to the interactions between the complex oxygen-containing functional groups in low-rank coal, the tensile vibrations of the C−O bond formed by the delocalization of the C−O and C═O bands in the carboxyl structure are not obvious.[39−41] In addition, the Na^+ of Na_2CO_3 and NaOH may convert the −COO on the surface of SL^+ into a resonance configuration; consequently, the absorption peaks near 1570 and 1400 cm^{-1} correspond to the asymmetric and symmetric stretching vibrations of the "−COONa" configuration, respectively. These results demonstrate that the Na^+ in NaCl solution will not interact with the carboxyl functional groups in the coal, whereas those in Na_2CO_3 and NaOH can react with these to form a "−COONa" structure.

3.1.4 XPS Analysis. XPS characterization was performed on coal samples to analyze the variations in the chemical state of the surface elements of the base SL^+ and treated samples, and the XPS spectra of sodium benzoate and sodium acetate was used for comparison (Figure 4). In Figure 4a, the peaks with binding energies around 283 and 531 eV are attributed to the characteristic peaks of C 1s and O 1s, respectively, while that around 1071 eV corresponds to that of Na 1s. The SL^+-NaCl

https://doi.org/10.1021/acsomega.1c03695
ACS Omega 2021, 6, 24848−24858

only shows the characteristic peaks of C and O elements, while SL^+-Na_2CO_3 and SL^+-NaOH show the characteristic peaks of Na in addition. The Na 1s spectra are shown in Figure 4b, where it can be seen that the binding energy positions of the characteristic peaks of Na in the SL^+-Na_2CO_3 and SL^+-NaOH samples are similar to those of sodium benzoate (1071.6 eV) and sodium acetate (1071.8 eV), indicating the bonding state of surface sodium and oxygen-containing functional groups of the two treated coal samples is similar to that of the "−COONa" configuration, which is consistent with the infrared characterization results.

In addition, Origin 8.5 data analysis software (OriginLab) was used to integrate the Na 1s peaks of the SL^+-Na_2CO_3 and SL^+-NaOH samples. The results indicated that the relative percentage of the "−COONa" configuration in the former was nearly 40% less than in the latter, indicating that sodium compounds with different properties form different amounts of "−COONa" with SL^+. The difference in the number of "−COONa" is also the main reason for the difference in combustion properties. Similar to the FT-IR results shown earlier, the XPS results further indicate that the Na^+ in NaCl solution will not interact with the carboxyl functional groups in the coal, whereas those from the Na_2CO_3 and NaOH solutions can form "−COONa" structure, with the number of such structures formed depending on the specific properties of the treating solution.

3.1.5 XRD Analysis. Figure 5 shows the XRD patterns of the base SL^+ and treated coal samples. As the figure shows, each sample clearly showed a wide diffraction peak in the range of 10−35°, indicating that the prepared coal was amorphous. As shown in Table 3, the SEM−EDS results indicated that sodium was present in the SL^+-Na_2CO_3 and SL^+-NaOH samples, but no characteristic peaks of sodium compounds were observed in the XRD pattern, implying that these compounds were either highly dispersed or bonded with organic oxygen-containing functional groups. The diffraction peak in the range of 10−35° is formed through the superposition of two peaks of γ and (002),[42,43] where the latter peak is located between 20 and 35°, corresponding to the distance between the spatial arrangement of the carbon network layer in the aromatic ring and the aromatic ring layer. The (002) peak of the coal samples is close to that of natural graphite (26°),[44] indicating that the lignite contains a certain amount of graphite-like structures. Peak fitting was performed on the diffraction peaks shown in Figure 5a (an example fitting diagram for the SL^+-NaCl sample is shown in Figure 5b), and the Bragg and Scherrer equations[43] were used to calculate the microcrystalline structural parameters of the coal sample such as the interplanar spacing of the aromatic layer, d_{002}, the size of the aromatic sheet layer, La, and the number of effective aromatic sheet layers, N. The results are shown in Table 4, where it can be seen that the interlayer spacing of the aromatic structures in the coal sample is larger than that of graphite (0.34 nm),[45] indicating that the coal samples have a low degree of graphitization and fewer microcrystalline structures. Compared to SL^+, the position of the (002) peak and the d_{002} of the SL^+-NaCl only changed slightly, whereas the d_{002} of the SL^+-Na_2CO_3 and SL^+-NaOH samples was significantly reduced; additionally, the value of La and N both increased. These results indicate the "−COOH" on the aromatic structure formed "−COONa" with Na, which affected the aromatic structure containing "−COOH", changed the order tropism of carbon in the coal, and further affected the reactivity of the aromatic structure. In conjunction with the FT-IR and XPS characterization results seen earlier, it may be inferred that the formation of a "−COONa" structure in the coal sample leads to the stabilization of the "−COOH" aromatic structure, thereby reducing its combustion reaction performance, and that the more "−COONa" present, the more stable the aromatic structure connected to it.

Table 4. Structural Parameters of the Carbon-Containing Microcrystalline Structure in the Base SL^+ and Treated Samples

samples	2θ (002)/°	d_{002}/nm	La/nm	N
SL^+	22.58	0.3935	1.512	2.760
SL^+-NaCl	22.69	0.3916	1.562	2.834
SL^+-Na_2CO_3	23.75	0.3743	1.673	2.950
SL^+-NaOH	23.95	0.3712	1.861	3.070

3.1.6 Raman Analysis. In order to further investigate the variations in the microstructure of the coal samples, Raman spectroscopy was carried out on the base SL^+ and treated samples. Figure 6a shows that the Raman spectra within the wavenumber range of 800−1800 cm^{-1} possessed two obvious characteristic peaks: the D peak located in the 1340−1380 cm^{-1} band, which is attributed to the presence of in-plane defects or heteroatoms such as vacancies, oxygen-containing groups, and other functional groups,[46,47] and the G peak in the 1580−1600 cm^{-1} band, which is attributed to the strong chemical bond formed by sp^2 hybridization of carbon atoms[48] and is largely caused by the graphite structure. In order to obtain the accurate positions and some of the important parameters related to the D and G peaks, a 4-peak Gaussian fit was performed on the Raman spectra[49] (Figure 6b shows a representative fitting diagram for the SL^+ sample), with the results shown in Table 4. Compared to SL^+, the positions of the D_1 and G peaks of the SL^+-NaCl sample were basically unchanged, while those of SL^+-Na_2CO_3 and SL^+-NaOH shifted to lower wavenumbers, with the latter showing a more pronounced shift. The shifts in the positions of the D_1 and G peaks are mainly caused by changes in the functional groups of the coal samples.[50] These results further indicate that the sodium, along with some of the organic matter (mainly oxygen-containing functional groups) in the coal formed a new structure during the treatment of SL^+ with the Na_2CO_3 and NaOH solutions. This finding is consistent with the FT-IR and XPS results presented earlier. In addition, the ratio of the areas of the D_1 and G peaks, I_{D1}/I_G, represents the degree of growth of aromatic rings, and increases with increasing degree of disorder.[51,52] Table 5 shows that the I_{D1}/I_G of SL^+-NaCl changed only slightly relative to SL^+, while those of the SL^+-Na_2CO_3 and SL^+-NaOH decreased significantly, with the latter showing the larger discrepancy with SL^+. This is due to the fact that in the NaOH treatment, more sodium ions bonded with organic functional groups compared to the Na_2CO_3 treatment, which lowered the degree of disorder of the sample to a larger extent and increased the stability of the aromatic structure containing "−COOH". Additionally, the crystal sizes of the microcrystalline planes, La, of the coal sample were calculated according to the intensities of the D_1 and G bands of the Raman spectra,[53] which showed that La increased with the alkalinity of the water-soluble sodium compounds. These results are consistent with the XRD characterization results discussed earlier.

https://doi.org/10.1021/acsomega.1c03695
ACS Omega 2021, 6, 24848−24858

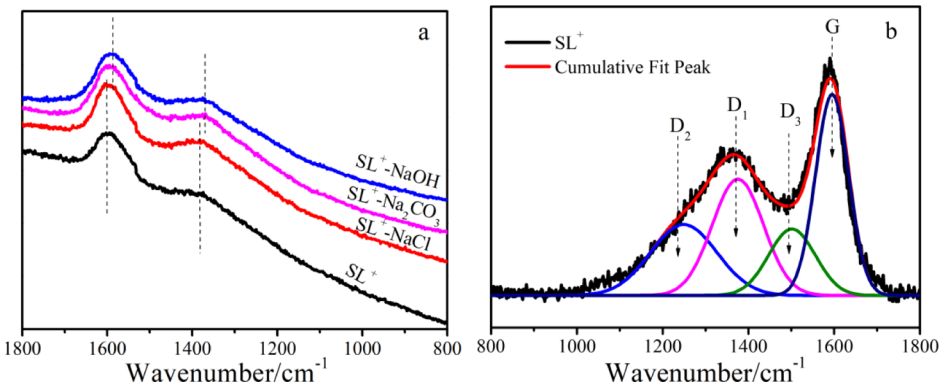

Figure 6. Raman spectra of base SL^+ and treated samples: (a) Raman spectra of coal samples; (b) peak-fitting diagram for SL^+.

Table 5. Parameters Obtained by Peak Fitting for the Base SL^+ and Treated Samples

samples	D_1/cm^{-1}	G/cm^{-1}	I_{D1}/I_G	La/nm
SL^+	1375	1595	0.8984	5.507
SL^+-NaCl	1375	1595	0.8892	5.574
SL^+-Na_2CO_3	1368	1588	0.7663	6.467
SL^+-NaOH	1356	1587	0.7484	6.622

3.2 Simulated Lignite with Carboxylic Compound.

The results presented thus far indicate that the "−COONa" structure formed by the carboxyl functional groups under the action of sodium ions can inhibit the combustion of lignite. Furthermore, the inhibitory effect is directly correlated with the number of "−COONa" present. Therefore, in order to further investigate the influence of the number of "−COONa" on combustion performance of lignite, the STMA-1, STMA-2, and STMA-3 samples (obtained by treating TMA with NaOH, as described in Section 2.2) were used.

3.2.1 FT-IR Analysis. Figure 7 shows the infrared spectra of the STMA samples, where it can be seen that the functional groups of the sample mainly change in the wavenumber range of 2000−400 cm^{-1}. TMA has an obvious carboxyl −C═O vibration absorption peak at 1720 cm^{-1}, which gradually decreases with increasing NaOH concentration. Once the concentration of NaOH reaches 3 mol/L, this peak basically disappears, indicating that the Na^+ in 3 mol/L NaOH can completely replace the hydrogen ions in the carboxyl group. Similar to the lignite samples treated with Na_2CO_3 and NaOH, the characteristic peaks for the −COO asymmetric and symmetric stretching vibrations of carboxylate appear at 1565 and 1370 cm^{-1} after treating TMA with NaOH, and become more obvious with increasing NaOH concentration. The peak at 613 cm^{-1} was attributed to the twisting vibrations of carboxyl −C═O, which is consistent with the variation of the absorption peak of the carboxyl group at 1720 cm^{-1}. With the increase in the NaOH concentration of the STMA samples, this peak weakens, disappearing completely in STMA-3. The peaks at 775 and 715 cm^{-1} result from the variable-angle vibrations of carboxylate, and their variation is consistent with those at 1565 and 1370 cm^{-1}. The absorption peaks at 775 and 715 cm^{-1} appear after NaOH treatment, becoming more prominent as the NaOH concentration increases.

3.2.2 Combustion Performance. Figure 8 shows the combustion performance curves of the STMA samples, where it can be seen that the main combustion peak of TMA is at ∼380 °C. For STMA-1, two additional combustion peaks appear at ∼440 and ∼480 °C, with the latter being the main peak. For STMA-2, the combustion peak at ∼380 °C disappears and the main combustion peak at ∼480 °C weakens, while a new peak appears at ∼560 °C. For STMA-3, only one combustion peak appears, at 558 °C. In conjunction with the FT-IR results, further analysis indicates that the carboxyl functional groups in STMA-3 bind the most sodium ions, which are believed to be mainly trisodium trimellitate. The combustion peaks of STMA-1 and STMA-2 in the temperature range of 420−550 °C are considered to be the main combustion peaks of the mixture of monosodium and disodium salts of TMA, which is similar to the TG results in the literature for mixtures of NaTP and Na_2TP prepared by adding different concentrations of NaOH to TP, as mentioned earlier.[51] Accordingly, it may be inferred that the peaks around 440, 480, and 560 °C correspond to the main combustion peaks of monosodium, disodium, and trisodium salts of TMA,

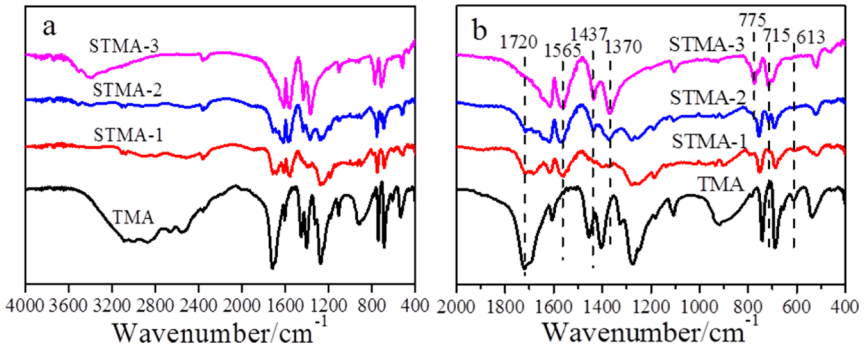

Figure 7. FT-IR spectra of the TMA and STMA samples in the wavenumber ranges of (a) 4000−400; (b) 2000−400 cm^{-1}.

https://doi.org/10.1021/acsomega.1c03695
ACS Omega 2021, 6, 24848−24858

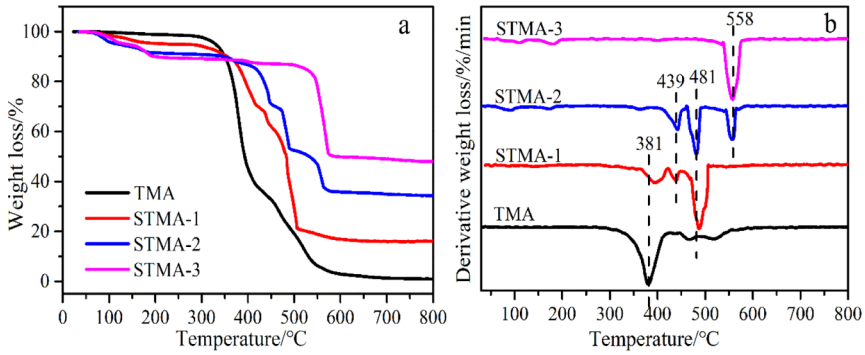

Figure 8. Combustion performance of TMA and STMA samples: (a) TG; (b) DTG.

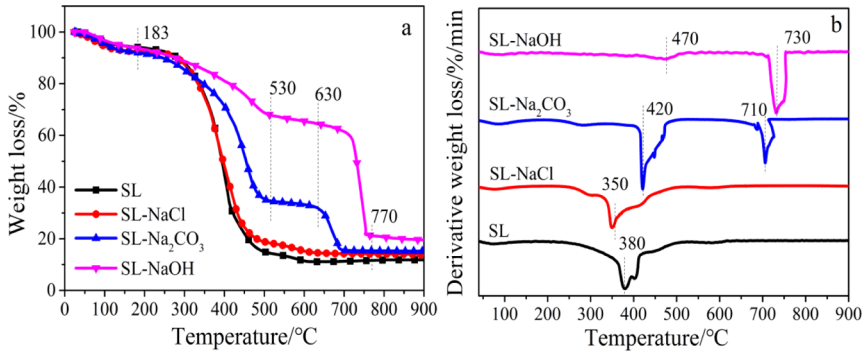

Figure 9. Combustion properties of the base SL and treated samples: (a) TG; (b) DTG.

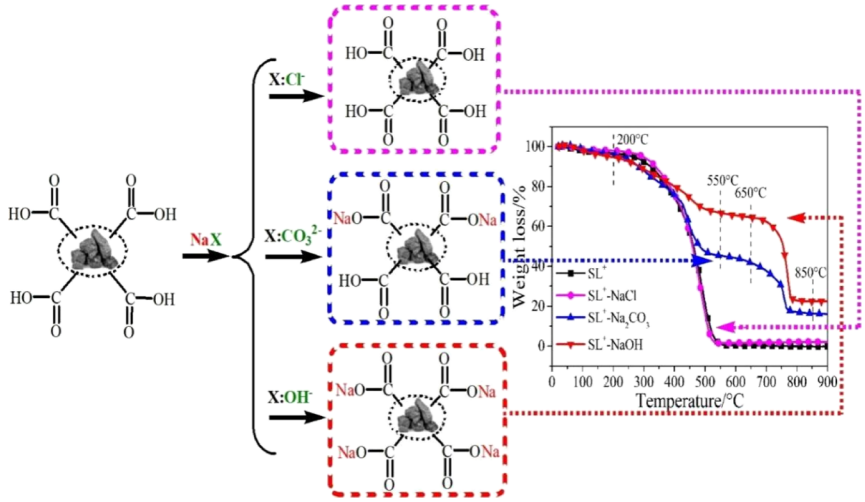

Figure 10. Structure−combustion performance relationship of the coal samples treated with different water-soluble sodium compounds.

respectively. The results are consistent with the changes in the combustion performance of lignite treated with different sodium compounds seen earlier in Section 3.1.1, further indicating that the higher the relative amount of "−COONa" formed, the greater the inhibitory effect on the combustion of lignite.

3.3 Verification Experiment. The above results were based on demineralized coal. In order to verify the effect of water-soluble sodium compound treatment on the combustion performance of lignite (SL), the same method as discussed before was used to conduct experiments on the action of Na_2CO_3 and NaOH on lignite. The results show that its combustion performance (Figure 9) is consistent with that of demineralized coal, which further illustrates that this treatment method is of practical significance for inhibiting the spontaneous combustion of lignite in reality.

3.4 Formation of "−COONa" in Coal Samples and the Mechanism of Action. As seen from the FT-IR and XPS results shown earlier, Na_2CO_3 and NaOH interact with the carboxyl functional groups in lignite to form different amounts of "−COONa" structure, the relative amount of which is directly correlated with the inhibition of lignite combustion. The reactions undergone by the lignite are similar to the formation of NaTP or Na_2TP from the interactions between the carboxyl group in TP and Na^+ ions.[34] They are also similar to the results for the STMA samples in Section 3.2. Combining the results obtained from this study, a possible structure-reaction relationship for the combustion of the Shengli lignite

https://doi.org/10.1021/acsomega.1c03695
ACS Omega 2021, 6, 24848−24858

treated with different water-soluble sodium compounds is proposed based on the complex structure of the lignite samples, as shown in Figure 10. The lignite samples treated with Na_2CO_3 and NaOH showed two weight-loss stages during the combustion process, which represent the combustion of different substances. The first of these is mainly caused by the loss of the inherent organic structure in the lignite, and the second is due to the combustion or decomposition of the "−COONa" structure formed in the lignite. As the relative amounts of "−COONa" formed in the lignite samples treated with these two compounds are different, their inhibitory effects on the combustion performance of lignite are accordingly different as well.

4. CONCLUSIONS

The effects of water-soluble sodium compounds with different properties on the structure and combustion performance of Shengli lignite were studied. The inhibitory effect of these compounds on the combustion performance of Shengli lignite mainly results from their alkalinity. Neutral NaCl did not cause significant variations in the combustion performance of the base lignite (SL^+), while the weakly alkaline Na_2CO_3 and strongly alkaline NaOH solutions did, of which the latter showed a stronger inhibitory effect on lignite combustion. The characterization results indicate that during treatment with Na_2CO_3 and NaOH, sodium interacts with the carboxyl oxygen-containing functional groups in lignite to form a "−COONa" structure, the higher stability of which leads to a significant increase in its main combustion temperature, and that the relative amount of "−COONa" is directly correlated with the inhibitory effect. The relative amount of "−COONa" formed by the Na_2CO_3 treatment was less than that formed by the NaOH treatment.

The results from this study, by shedding light on the mechanisms of lignite treatment by alkaline solutions, are of practical significance toward inhibiting the spontaneous combustion of lignite in real-world situations and thereby boosting its safe and effective utilization.

AUTHOR INFORMATION

Corresponding Authors

Runxia He − *Inner Mongolia Key Laboratory of High-Value Functional Utilization of Low Rank Carbon Resources, College of Chemical Engineering, Inner Mongolia University of Technology, Huhhot, Inner Mongolia 010051, China;* orcid.org/0000-0001-7357-3043; Phone: +86 13664742350; Email: runxiahe@imut.edu.cn

Quansheng Liu − *Inner Mongolia Key Laboratory of High-Value Functional Utilization of Low Rank Carbon Resources, College of Chemical Engineering, Inner Mongolia University of Technology, Huhhot, Inner Mongolia 010051, China;* orcid.org/0000-0001-7763-7569; Phone: +86 13664740405; Email: liuqs@imut.edu.cn

Authors

Yanjun Wang − *Inner Mongolia Key Laboratory of High-Value Functional Utilization of Low Rank Carbon Resources, College of Chemical Engineering, Inner Mongolia University of Technology, Huhhot, Inner Mongolia 010051, China*

Yunfei Zhao − *Inner Mongolia Key Laboratory of High-Value Functional Utilization of Low Rank Carbon Resources, College of Chemical Engineering, Inner Mongolia University of Technology, Huhhot, Inner Mongolia 010051, China*

Zhenghao Yan − *Inner Mongolia Key Laboratory of High-Value Functional Utilization of Low Rank Carbon Resources, College of Chemical Engineering, Inner Mongolia University of Technology, Huhhot, Inner Mongolia 010051, China*

Xuemei Li − *Inner Mongolia Key Laboratory of High-Value Functional Utilization of Low Rank Carbon Resources, College of Chemical Engineering, Inner Mongolia University of Technology, Huhhot, Inner Mongolia 010051, China*

Huacong Zhou − *Inner Mongolia Key Laboratory of High-Value Functional Utilization of Low Rank Carbon Resources, College of Chemical Engineering, Inner Mongolia University of Technology, Huhhot, Inner Mongolia 010051, China;* orcid.org/0000-0002-9137-4694

Na Li − *Inner Mongolia Key Laboratory of High-Value Functional Utilization of Low Rank Carbon Resources, College of Chemical Engineering, Inner Mongolia University of Technology, Huhhot, Inner Mongolia 010051, China*

Keduan Zhi − *Inner Mongolia Key Laboratory of High-Value Functional Utilization of Low Rank Carbon Resources, College of Chemical Engineering, Inner Mongolia University of Technology, Huhhot, Inner Mongolia 010051, China*

Yinmin Song − *Inner Mongolia Key Laboratory of High-Value Functional Utilization of Low Rank Carbon Resources, College of Chemical Engineering, Inner Mongolia University of Technology, Huhhot, Inner Mongolia 010051, China*

Yingyue Teng − *Inner Mongolia Key Laboratory of High-Value Functional Utilization of Low Rank Carbon Resources, College of Chemical Engineering, Inner Mongolia University of Technology, Huhhot, Inner Mongolia 010051, China*

Complete contact information is available at: https://pubs.acs.org/10.1021/acsomega.1c03695

Author Contributions

†Y.W. and Y.Z. are contributed equally to this work.

Notes

The authors declare no competing financial interest.

ACKNOWLEDGMENTS

The authors greatly acknowledge the financial support from the National Natural Science Foundation of China (21566028, 21766023, 21868021, and 21968021), the Science and Technology Plan Project of Inner Mongolia (2020GG0289), and the Natural Science Foundation of Inner Mongolia (2019MS02025 and 2020MS02023).

REFERENCES

(1) Khan, M. Z.; Chun, D. H.; Yoo, J.; Kim, S. D.; Rhim, Y. J.; Choi, H. K.; Lim, J.; Lee, S.; Rifella, A. Evaluation of the effect of a palm acid oil coating on upgrading low rank coal. *RSC Adv.* **2015**, *5*, 63955−63963.

(2) Cheng, G.; Li, Z.; Ma, Z.; Cao, Y.; Sun, L.; Jiang, Z. Optimization of collector and its action mechanism in lignite flotation. *Powder Technol.* **2019**, *345*, 182−189.

(3) Zhang, B.; Chen, Y. L. Particle size effect on pore structure characteristics of lignite determined via low-temperature nitrogen adsorption. *J. Nat. Gas Sci. Eng.* **2020**, *84*, 103633.

(4) Wei, F.; Liao, J.; Chang, L.; Han, Y.; Bao, W. Transformation of functional groups during lignite heat-treatment and its effects on moisture re-adsorption properties. *Fuel Process. Technol.* **2019**, *192*, 210−219.

(5) Saikia, B. K.; Boruah, R. K.; Gogoi, P. K. FT-IR and XRD analysis of coal from Makum coalfield of Assam. *J. Earth Syst. Sci.* **2007**, *116*, 575−579.
(6) Cui, F.-S.; Laiwang, B.; Shu, C.-M.; Jiang, J.-C. Inhibiting effect of imidazolium-based ionic liquids on the spontaneous combustion characteristics of lignite. *Fuel* **2018**, *217*, 508−514.
(7) Wang, H.; Dlugogorski, B. Z.; Kennedy, E. M. Coal oxidation at low temperatures: oxygen consumption, oxidation products, reaction mechanism and kinetic modelling. *Prog. Energy Combust. Sci.* **2003**, *29*, 487−513.
(8) Fei, Y.; Aziz, A. A.; Nasir, S.; Jackson, W. R.; Marshall, M.; Hulston, J.; Chaffee, A. L. The spontaneous combustion behavior of some low rank coals and a range of dried products. *Fuel* **2009**, *88*, 1650−1655.
(9) Zhao, J.; Deng, J.; Song, J.; Shu, C.-M. Effectiveness of a high-temperature-programmed experimental system in simulating particle size effects on hazardous gas emissions in bituminous coal. *Saf. Sci.* **2019**, *115*, 353−361.
(10) Cheng, W.; Hu, X.; Xie, J.; Zhao, Y. An intelligent gel designed to control the spontaneous combustion of coal: Fire prevention and extinguishing properties. *Fuel* **2017**, *210*, 826−835.
(11) Qiao, L.; Deng, C.; Dai, F.; Fan, Y. Experimental study on a metal-chelating agent inhibiting spontaneous combustion of coal. *Energy Fuels* **2019**, *33*, 9232−9240.
(12) Watanabe, W. S.; Zhang, D.-k. The effect of inherent and added inorganic matter on low-temperature oxidation reaction of coal. *Fuel Process. Technol.* **2001**, *74*, 145−160.
(13) Lu, W.; Guo, B. L.; Qi, G. S.; Cheng, W. M.; Yang, W. Y. Experimental study on the effect of preinhibition temperature on the spontaneous combustion of coal based on an $MgCl_2$ solution. *Fuel* **2020**, *265*, 117032.
(14) Tang, Y. Inhibition of low-tmperature oxidation of bituminous coal using a novel phase-transition aerosol. *Energy Fuels* **2016**, *30*, 9303−9309.
(15) Qi, X.; Wei, C.; Li, Q.; Zhang, L. Controlled-release inhibitor for preventing the spontaneous combustion of coal. *Nat. Hazards* **2016**, *82*, 891−901.
(16) Li, J. L.; Lu, W.; Xu, J. Coal spontaneous combustion prevention and cure with chemical retarder as well as analysis on retarding mechanism. *Coal Sci. Technol.* **2012**, *40*, 50−53.
(17) Deng, J.; Lü, H.-F.; Xiao, Y.; Wang, C.-P.; Shu, C.-M.; Jiang, Z.-G. Thermal effect of ionic liquids on coal spontaneous combustion. *J. Therm. Anal. Calorim.* **2019**, *138*, 3415−3424.
(18) Lei, Z.-P.; Cheng, L.-L.; Zhang, S.-F.; Zhang, Y.-Q.; Shui, H.-F.; Ren, S.-B.; Wang, Z.-C. Dissolution performance of coals in ionic liquid 1-butyl-3-methyl-imidazolium chloride. *Fuel Process. Technol.* **2015**, *129*, 222−226.
(19) Xi, X.; Shi, Q.; Jiang, S.; Zhang, W.; Wang, K.; Zhengyan, W. Study on the effect of ionic liquids on coal spontaneous combustion characteristic by microstructure and thermodynamic. *Process Saf. Environ. Protect.* **2020**, *140*, 190−198.
(20) Zhan, J.; Wang, H.-H.; Song, S.-N.; Hu, Y.; Li, J. Role of an additive in retarding coal oxidation at moderate temperatures. *Proc. Combust. Inst.* **2011**, *33*, 2515−2522.
(21) Geng, W.; Nakajima, T.; Takanashi, H.; Ohki, A. Analysis of carboxyl group in coal and coal aromaticity by Fourier transform infrared (FT-IR) spectrometry. *Fuel* **2009**, *88*, 139−144.
(22) Wang, D.; Dou, G.; Zhong, X.; Xin, H.; Qin, B. An experimental approach to selecting chemical inhibitors to retard the spontaneous combustion of coal. *Fuel* **2014**, *117*, 218−223.
(23) Bai, Z.; Wang, C.; Deng, J.; Kang, F.; Shu, C.-M. Experimental investigation on using ionic liquid to control spontaneous combustion of lignite. *Process Saf. Environ. Protect.* **2020**, *142*, 138−149.
(24) Nasir, S.; Sarfaraz, T. B.; Verheyen, T. V.; Chaffee, A. L. Structural elucidation of humic acids extracted from Pakistani lignite using spectroscopic and thermal degradative techniques. *Fuel Process. Technol.* **2011**, *92*, 983−991.
(25) Liu, X.; Feng, L.; Song, L.; Wang, X.; Zhang, Y. Effect of NaOH treatment on combustion performance of Xilinhaote lignite. *Int. J. Min. Sci. Technol.* **2014**, *24*, 51−55.
(26) Wang, D.; He, R.; Wang, B.; Zhou, H.; Song, Y.; Zhi, K.; Chen, J.; Li, N.; Ban, Y.; Liu, Q. Effects of alkali-oxygen oxidation temperature on the structures and combustion properties of Shengli lignite. *RSC Adv.* **2017**, *7*, 19833−19840.
(27) Sathe, C.; Pang, Y.; Li, C.-Z. Effects of heating rate and ion-exchangeable cations on the pyrolysis yields from a Victorian brown coal. *Energy Fuels* **1999**, *13*, 748−755.
(28) Li, C. Z.; Sathe, C.; Kershaw, J. R.; Pang, Y. Fates and roles of alkali and alkaline earth metals during the pyrolysis of a Victorian brown coal. *Fuel* **2000**, *79*, 427−438.
(29) Wei, X. F.; Liu, T. F.; Huang, J. J.; Fang, Y. T.; Wang, Y. Transformation of Na in an Australian high-sodium coal during pyrolysis. *J. Fuel Chem. Technol.* **2010**, *38*, 144−148.
(30) Liu, D.; Zhang, S.; Tu, S.; Jin, T.; Shi, D.; Pei, Y. Transformation of sodium during Wucaiwan coal pyrolysis. *J. Fuel Chem. Technol.* **2014**, *42*, 1190−1196.
(31) Xu, L.; Liu, H.; Fang, H.; Gao, J.; Wu, S. Effects of various inorganic sodium salts present in Zhundong coal on the char characteristics. *Fuel* **2017**, *203*, 120−127.
(32) Sánchez, N. M.; de Klerk, A. Oxidative ring-opening of aromatics: Thermochemistry of sodium, potassium and magnesium biphenyl carboxylates. *Thermochim. Acta* **2016**, *645*, 31−42.
(33) Yan, Z.; Chen, J.; He, R.; Li, N.; Zhou, H.; Song, Y.; Ban, Y.; Zhi, K.; Teng, Y.; Liu, Q. Suppression of crosslinking combination of carboxyl functional groups with NaOH on combustion performance of Shengli lignite. *Fuel* **2018**, *227*, 13−20.
(34) Park, Y.; Shin, D.-S.; Woo, S. H.; Choi, N. S.; Shin, K. H.; Oh, S. M.; Lee, K. T.; Hong, S. Y. Sodium Terephthalate as an Organic Anode Material for Sodium Ion Batteries. *Adv. Mater.* **2012**, *24*, 3562−3567.
(35) Wang, Y.; Xue, S.; Tang, Y.; Mei, F.; He, W.; Pan, H. Effect of NaOH Treatment on the Low-Temperature Oxidation Behavior of Lignite. *Energy Fuels* **2019**, *33*, 9161−9170.
(36) Parsa, M. R.; Tsukasaki, Y.; Perkins, E. L.; Chaffee, A. L. The effect of densification on brown coal physical properties and its spontaneous combustion propensity. *Fuel* **2017**, *193*, 54−64.
(37) Parsa, M. R.; Chaffee, A. L. The effect of densification with NaOH on brown coal thermal oxidation behaviour and structure. *Fuel* **2018**, *216*, 548−558.
(38) Parsa, M. R.; Chaffee, A. L. The effect of densification with alkali hydroxides on brown coal self-heating behaviour and physico-chemical properties. *Fuel* **2019**, *240*, 299−308.
(39) Ban, Y. P.; Liu, Q. S.; Zhou, H. C.; Li, N.; Zhao, B. Q.; Shi, S. L.; He, R. X.; Zhi, K. D. Catalytic effect of representative calcium salts on the steam gasification of a Shengli lignite. *Fuel* **2019**, *255*, 115832.
(40) Manoj, B.; Narayanan, P. Study of changes to the organic functional groups of a high volatile bituminous coal during organic acid treatment process by FTIR spectroscopy. *J. Miner. Mater. Charact. Eng.* **2013**, *01*, 39−43.
(41) Ban, Y. P.; Wang, Y.; Li, N.; He, R. X.; Zhi, K. D.; Liu, Q. S. The catalytic effect of calcium and potassium on CO_2 gasification of Shengli lignite: the role of carboxyl. *R. Soc. Open Sci.* **2018**, *5*, 180717.
(42) Xiong, Y. K.; Jin, L. J.; Yang, H.; Li, Y.; Hu, H. Q. Insight into the aromatic ring structures of a low-rank coal by step-wise oxidation degradation. *Fuel Process. Technol.* **2020**, *210*, 106563.
(43) Xin, F. D.; Xu, H.; Tang, D. Z.; Cao, L. K. Properties of lignite and key factors determining the methane adsorption capacity of lignite: New insights into the effects of interlayer spacing on adsorption capacity. *Fuel Process. Technol.* **2019**, *196*, 106181.
(44) Hou, D.; Li, K.; Ma, R.; Liu, Q. Influence of order degree of coaly graphite on its structure change during preparation of graphene oxide. *J Materiomics* **2020**, *6*, 628−641.
(45) Zhang, S.; Liu, Q.; Zhang, H.; Ma, R.; Li, K.; Wu, Y.; Teppen, B. J. Structural order evaluation and structural evolution of coal derived natural graphite during graphitization. *Carbon* **2020**, *157*, 714−723.

https://doi.org/10.1021/acsomega.1c03695
ACS Omega 2021, 6, 24848−24858

(46) Ferrari, A. C.; Robertson, J. Interpretation of Raman spectra of disordered and amorphous carbon. *Phys. Rev. B: Condens. Matter Mater. Phys.* **2000**, *61*, 14095−14107.
(47) Ferreira, E. H. M.; Moutinho, M. V. O.; Stavale, F.; Lucchese, M. M.; Capaz, R. B.; Achete, C. A.; Jorio, A. Evolution of the Raman spectra from single-, few-, and many-layer graphene with increasing disorder. *Phys. Rev. B: Condens. Matter Mater. Phys.* **2010**, *82*, 125429.
(48) Chen, W.; Jiao, N.; Xu, L.; Cao, W. Transition of sp^2 hybridization structure during graphitization of carbon fiber. *Aerosp. Mater. Technol.* **2013**, *43*, 46−48.
(49) Chabalala, V. P.; Wagner, N.; Potgieter-Vermaak, S. Investigation into the evolution of char structure using Raman spectroscopy in conjunction with coal petrography; Part 1. *Fuel Process. Technol.* **2011**, *92*, 750−756.
(50) Li, X. J.; Li, C. Z. Volatilisation and catalytic effects of alkali and alkaline earth metallic species during the pyrolysis and gasification of Victorian brown coal. Part VIII. Catalysis and changes in char structure during gasification in steam. *Fuel* **2006**, *85*, 1518−1525.
(51) Qin, Y.-h.; Han, Q.-q.; Zhao, Z.-b.; Du, Z.-y.; Feng, J.; Li, W.-y.; Vassilev, S. V.; Vassileva, C. G. Impact of biomass addition on organic structure and mineral matter of char during coal-biomass co-gasification under CO_2 atmosphere. *Fuel* **2017**, *202*, 556−562.
(52) Flahaut, E.; Laurent, C.; Peigney, A. Catalytic CVD synthesis of double and triple-walled carbon nanotubes by the control of the catalyst preparation. *Carbon* **2005**, *43*, 375−383.
(53) Sonibare, O. O.; Haeger, T.; Foley, S. F. Structural characterization of Nigerian coals by X-ray diffraction, Raman and FTIR spectroscopy. *Energy* **2010**, *35*, 5347−5353.

https://doi.org/10.1021/acsomega.1c03695
ACS Omega 2021, 6, 24848−24858